Ceramics-Silikáty 67 (2), 135-141 (2023)
www.ceramics-silikaty.cz doi: 10.13168/cs.2023.0010

THE EFFECT OF THE PRE-CRYSTALLISATION DEFECT SIZE ON THE STRENGTH LIMITATION IN LITHIUM SILICATE GLASS CERAMICS

#KRISTÝNA HYNKOVÁ*, **, HAI-LIN DENG***, IVA VOBORNÁ**

*School of Dentistry, University of Alberta, Edmonton Clinic Health Academy, 11405 87 Avenue NW, Edmonton T6G 1C9, AB, Canada
**Faculty of Medicine and Dentistry, Palacký University, Palackého 12, Olomouc 772 00, Czech Republic
***Department of Mechanics, Sichuan University, Chengdu 610065, China

#E-mail: kristyna.hynkova01@upol.cz

Submitted February 6, 2023; accepted March 18, 2023

Keywords: Lithium silicate, Dental glass ceramic, Crystallisation, Surface defects, Bi-axial flexural strength

The objective of this study was to explore how the size of pre-crystallisation defects affects the strength of a lithium disilicate glass ceramic. A total of seven groups of lithium disilicate glass-ceramic (IPS e.max® CAD) disc shape specimens (thickness 1.1 ± 0.1mm) were fabricated (n = 15). Each group corresponded to the varying severity of controlled surface defects made by a Vickers hardness indenter in a partially crystallised state. All the discs followed the manufacturer specified crystallisation process. The controlled defects were analysed with the use of optical microscopy and atomic force microscopy in both the partially crystallised phase and after crystallisation. The bi-axial flexural strength (BFS) was measured using a ball-on-ring configuration after crystallisation. A one-way ANOVA revealed a significant difference (p = 0.028). The post-hoc Tukey test revealed a significant difference (p < 0.01) existed between the 0.2 kg and 2 kg indentation groups, with no other pairwise differences. The survivability plots highlight the low BFS outliers occurring in the 1.0 and 2.0 kg static load groups. The Atomic Force Microscopy shows apparent differences before and after crystallisation. The crystallisation process helps to mitigate the strength limiting defects, but it also has a limit. Therefore, it is necessary to minimise the surface defects generated through the pre-crystallisation manufacturing procedures.

INTRODUCTION

The rise in popularity of Computer Aided Design/Computer Aided Manufacture (CAD/CAM) in dental applications has resulted in more efficient workflows for professionals and reduced overall treatment times, benefiting both the patient and clinicians. The production of ceramic restorations primarily involves subtractive machining. During this grinding process, material is removed from pre-formed ceramic blocks using abrasives, typically embedded diamond particles, to achieve the required shape of the dental restoration [1, 2].

There are two main approaches in the literature with regards to the grinding analysis: i) the "machining" approach ii) "indentation fracture mechanics" [3]. The machining approach assumes a role of a plastic-flow mode of chip formation after the grain penetrates a critical depth. For ceramic materials, the plastic-flow regime is negligible and, thus, the fracture mechanics approach is typically pursued for ceramic materials, where it has been shown to be a reasonable model to describe the material removal process [3].

Indentation fracture mechanics analyses the micro-fractures and material loss as a result of the localised stress concentration caused by the diamond particles [4, 5]. This contact between the abrasive and the material results in strength limiting cracks and plastic contact damage leading to residual stresses localised within a region near the machined surface [3-6]. While the grinding/indentation processes involve both elastic and plastic fields formed by the indenter, the elastic component only plays a role during the formation of cracks as it fully reverses. On the other hand, the plastic field is irreversible, and the associated residual field affects both the formation of the cracks as well as their response to the subsequent loading [7, 8]. Instead of failure occurring at a critical applied stress without a precursor crack extension (as is the case for Griffith cracks) [9], the cracks become unstable only after a region of stable equilibrium growth [10, 11].

Cracks induced by this contact can be classified into two primary systems: i) lateral cracks, formed normal to the grinding direction; ii) median cracks, formed parallel to the grinding direction (Figure 1) [6-8, 12, 13].

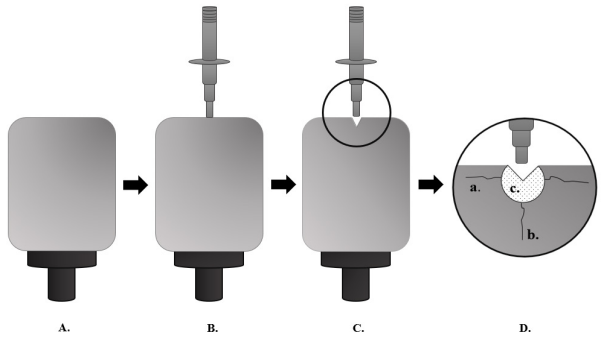

Figure 1. Illustration of the subtractive machining process. (A) Ceramic block. (B) Diamond tool in contact with the ceramic block. (C) Ground sulcus. (D) (a) lateral cracks (D) (b) median cracks (D) (c) plastic deformation zone under the sulcus.

Lateral cracks play a dominant role in the chipping of the material, while median cracks deteriorate the strength of the material when they are more severe than the pre-existing cracks in the material.

There are two primary types of CAD/CAM ceramic materials available on the market with respect to the crystallisation process i) fully or ii) partially crystallised systems. Fully crystallised ceramics are obtained and machined in their (already) fully crystalised state. Partially crystallised ceramics are further crystallised after the machining process. While the partially crystallised system process is more economically demanding and more time consuming, it is favourable for machining as the material is softer, it has better edge stability and causes less wear of the burs [14-16]. After machining, the material undergoes a heating process (crystallisation), reaching its final microstructure and mechanical, physical, and optical properties [14, 15, 17-21]. Furthermore, this process has been shown to have crack-healing properties [15]. This study focuses on the positive effects (in terms of crack healing and strength improvement) of crystallisation for the partially crystallised IPS e.max® CAD ceramics.

There are multiple material processes during the crystallisation that can be potentially beneficial to the introduced defects and resulting strength degradation. As the glass exceeds the transition temperature during heating, it gets into a viscous state without losing its shape [22]. This process (also referred to as annealing) also relieves any residual stresses initially present in the material [23]. The crystallisation process also changes the ceramic crystalline microstructure. The IPS e.max® CAD block in the partially crystalline stage mainly consists of i) few lithium disilicate crystals ii) amorphous lithium orthophosphate which acts as nucleation agent iii) metasilicate crystals occupying the majority of the material [14, 18, 24, 25]. As the temperature reaches 530 °C, the metasilicate crystals grow with dendritic shape, reaching their maximum size at around 750 °C. The metasilicate crystals (Li_2SiO_3) then start decomposing above 780 °C until 820 °C. The formations of the main crystal phase of lithium di-silicate ($Li_2Si_2O_5$) and a second crystal phase of lithium orthophosphate (Li_3PO_4) follow [19, 24, 25]. While $Li_2Si_2O_5$ crystals are also formed under lower temperatures in parallel with the metasilicate growth, their faster and major formation happens only after the decomposition of the metasilicate crystals and their interactions with glass. $Li_2Si_2O_5$ crystals reach 70 % volume in a fully crystalised stage and can be found in two different morphologies i) rod-like crystals ii) oriented crystals. Rod-like crystals are formed during the decomposition of metasilicate crystals and their subsequent interaction with silicate in a rich glass viscous matrix. The oriented crystal bundle forms a rearrangement of a silicate framework in Li_2SiO_3 [14, 17, 20, 26]. The structural changes during the crystallisation process are graphically shown in Figure 2.

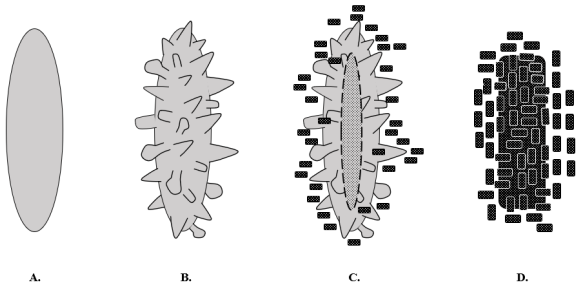

Figure 2. Illustration of lithium silicate crystals during the crystallisation process. (A) Plate metasilicate crystal. (B) Dendritic metasilicate crystal (C). Dendritic metasilicate crystal in decomposition with a formation of bundle and rod-like lithium di-silicate crystals (D) Fully crystalised lithium di-silicate crystals with a bundle-crystal form in the centre and rod-like crystals around it.

While previous work has demonstrated that the crystallisation process does decrease the crack dimensions introduced during machining, the resulting defects were still strength limiting [15]. However, only a single defect severity was considered. The effects of the crystallisation process on the varying defect sizes and the resulting strength degradation are, thus, not well understood.

The aim of this study is to determine the effect of the crystallisation process on defects of varying severities in a partially crystallised lithium disilicate CAD/CAM ceramic. The hypothesis is that the crystallisation process can mitigate the defects within a critical size, in terms of the strength limitation.

EXPERIMENTAL

Test specimen manufacturing

This study used partially crystallised lithium disilicate ceramic IPS e.max® CAD blocks (Ivoclar Vivadent, Schaan, Litchenstein). In accordance with previous studies, the blocks were cut with a water jet into cylinder shapes with a nominal diameter of 10 mm [27, 28]. A slow speed linear precision saw with a diamond particle cutting blade IsoMet 5000 (Buehler, Lake Bluff, USA) with water lubrication was used to cut 105-disc samples measuring 1.1 ± 0.1 mm in thickness. The parameters used were a blade speed of 4000 rpm, a feed rate of 19 mm·min^{-1}, a blade thickness of 0.508 mm. One side of the ceramic disc was polished to reach a consistent surface finish on which to impose defects. All the samples were polished by hand, using silicon carbide abrasive paper in a progression of P-800, P-1000, P-1500, and P-2000 at 90 s intervals on each disc. Water was used as the lubricant during polishing.

Controlled Defect Generation

The samples were randomly categorised into 7 groups (n = 15 per group), corresponding to the different indentation loads. The controlled surface defects were made by indentation with a Vickers hardness indenter (Wilson® Vickers Micro-hardness Tester, Buehler, Lake Bluff, USA). In order to simulate the varying severities of the surface defects, each group used a different static load of the microhardness indentation: Group CONT, control group (polish); Group IND0.1, indent with 0.1 kg; Group IND0.2, indent with 0.2 kg; Group IND0.3, indent with 0.3 kg; Group IND0.5, indent with 0.5 kg; Group IND1, indent with 1.0 kg; Group IND2, indent with 2.0 kg. All static loads were held for 99 s. To make the location of the indentation consistent, the approximate centre of all the discs was identified using a 3D printed locator.

Crystallisation

All the samples were subjected to the crystallisation process in an Ivoclar Vivadent Programat EP 5000 furnace, as specified by the manufacturer. This process consisted of the following schedule: 1) preheating samples to 403 °C for 6 min, 2) increasing the temperature at 90 °C·min^{-1} to 820 °C (550° - 820 °C under a vacuum), 3) holding for 0.1 minute, 4) increasing 30 °C·min^{-1} to 840 °C, 5) holding for 7 minutes, 6) long-term cooling from 700 °C. After the crystallisation process, the thicknesses of the samples were re-measured.

Optical and Atomic Force Microscopy

The indented surface of the samples was observed with an optical microscope (50 × zoom) attached to a Wilson® Micro-hardness tester (Buehler, Lake Bluff, USA) before and after the crystallisation process. The optical microscope was used to measure the cracks and indentation that form the surface defects (Figure 3). The crack size was measured as a sum of the horizontal/vertical crack lengths and the indent size was measured as the horizontal/vertical dimensions of the diamond rhomb (Figure 3).

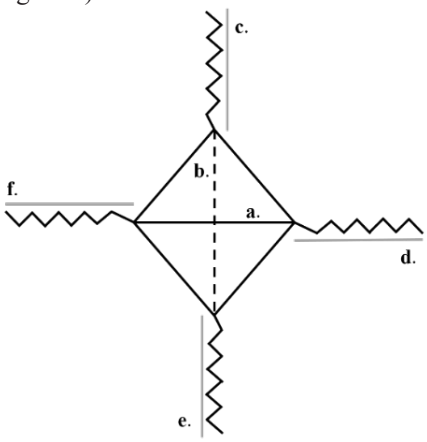

Figure 3. Illustration of the microcracks and indentation. The diamond shape represents the Vickers indentation with a horizontal/vertical length of a/b. Four lateral microcracks propagating from the corners are marked as c, d, e, f.

Whenever any of these values were not recognisable (e.g., at lower static indenter loads where propagating cracks could not be discerned), the datapoint was removed in order not to bias the data. As the crystallisation process resulted in substantial changes to the diamond indent geometry, the measurements were performed prior to the crystallisation only.

To further observe the effect of the crystallisation process on the surface defects, Atomic Force Microscopy (AFM) was performed. Six additional samples were made: two samples were just polished, and four were exposed to Vickers indents with two at a 0.5 kg static load and at 2.0 kg. The AFM was performed before and after the crystallisation process, using a Dimension Edge AFM (Bruker, Billerica, USA), using a Tap300-G (Ted Pella Inc, Redding, USA) silicone probe in a tapping mode, with a scan size of 50 × 50 μm and scan rate of 0.5 Hz.

Bi-axial flexural strength (BFS) determination

The BFS was measured using a ball on ring biaxial flexure configuration and a universal testing machine (ElectroPuls E 3000, Instron, Norwood, USA). The disc shape specimens were supported on a knife edge ring (diameter of 8.3 mm) and were loaded centrally with a stainless-steel ball indenter (diameter of 7.9 mm) at a cross head speed of 1 mm·min^{-1}. The polished/indented surface of the samples was facing down (i.e., facing the ring) to load the effected surface in tension. The

resulting BFS was calculated using the Timoshenko and Woinowsky Krieger formulation (Equation 1)

$$BFS = \frac{P}{h^2} \times \left[(1+v) \times \left[0.485 \times ln\ ln\ \left(\frac{a}{h}\right) + 0.52\right] + 0.48\right] \quad (1)$$

where P is the force at fracture (N), v is Poison's ratio for the material (v = 0.215 for IPS e.max® CAD), a is the radius of the knife-edge supporter (mm), and h is the sample thickness.

Statistical analysis

The Kolmogorov-Smirnov test was used to test the data normality. A one-way analysis of variance (ANOVA) test was used to test for a significant difference in the mean BFS values of all the groups (CONT; IND 0.1; IND 0.2; IND 0.3; IND 0.5; IND 1; IND 2). The post-hoc Tukey test was then used for the pairwise comparison to determine significance differences between any individual group pairs. All the statistical tests were applied with a significance level of a = 0.05.

RESULTS

The minimum and maximum BFS values, mean BFS and associated standard deviations for all the experimental groups are summarised in Table 1 and Figure 4. The Kolmogorov-Smirnov test did not reject normality. The one-way ANOVA (a = 0.05) revealed a significant difference (p = 0.028). The post-hoc Tukey test (a = 0.05) determined a significant difference between the groups IND 0.2 and IND 2 (p < 0.01).

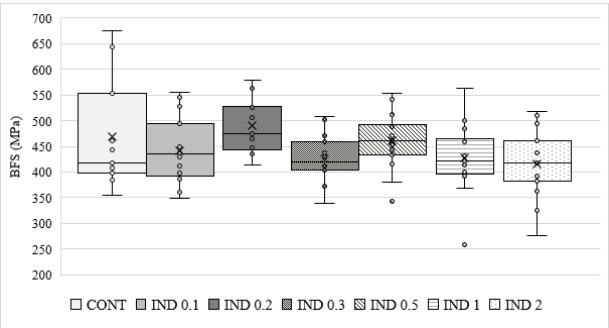

Figure 4. Box plot graph of the BFS values. BFS value (MPa) with the mean/standard deviation and inner/outlier points.

A BFS plot of the survival probability was made to further analyse the differences between the groups, as shown in Figure 5.

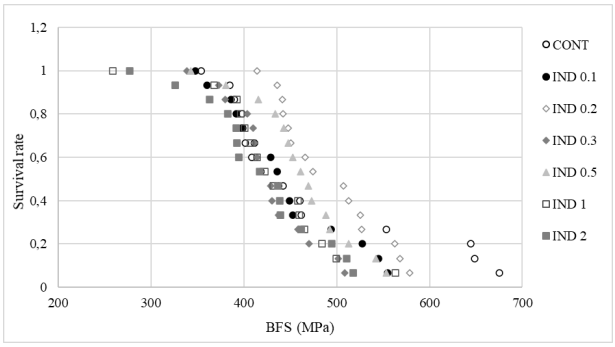

Figure 5. The survival rate of the tested samples under different BFS values. The groups with the largest surface defects IND 1 and IND 2 (1 kg and 2 kg loads) demonstrate discontinuity in the lowest BFS values, being the only ones that survived less than 300 MPa.

The groups with the two largest defect sizes, IND1 and IND2, exhibit outliers at lower strength values, suggesting the limit of the crystallisation process, where the only samples with a BFS below 300 MPa come from these two groups (Figure 6-7).

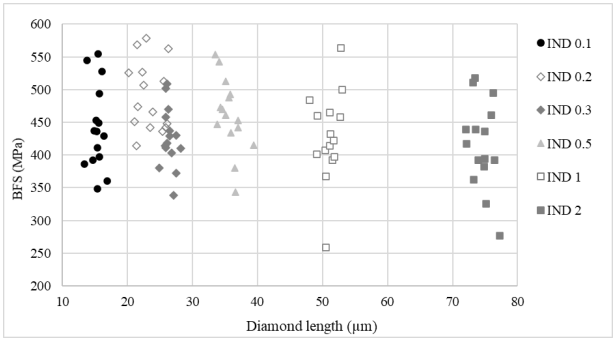

Figure 6. Diamond length against the BFS. The different indentation loads (different groups) clearly affect the size of the defect. Only samples with an intelligible diamond length were included.

Figure 6 and Figure 7 relate the defect severity to the BFS. Figure 6 focuses on the size of the diamond, while Figure 7 focuses on the crack dimensions propagating from the central Vickers indent. The figures demonstrate that the indentation load correlates with the defect severity, as the groups form identifiable clusters.

Table 1. Table 1- BFS values: mean and standard deviations.

Group	CONT (control)	IND 0.1 (0.1 kg)	IND 0.2 (0.2 kg)	IND 0.3 (0.3 kg)	IND 0.5 (0.5 kg)	IND 1 (1 kg)	IND 2 (2 kg)
BFS (MPa)	354 - 675	348 – 555	414 - 578	339 - 508	343 – 553	259 - 564	277 - 517
Mean BFS (MPa)	469 ± 104	441 ± 62	490 ± 52	426 ± 44	461 ± 54	428 ± 66	416 ± 64

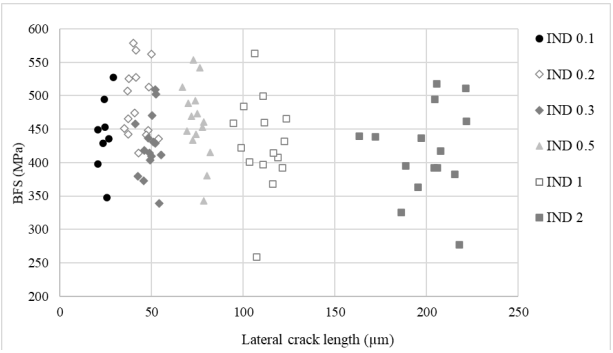

Figure 7. Lateral crack size against the BFS. The different indentation loads (different groups) clearly affect the crack length of the defect. Only samples with an intelligible diamond length were included.

To inspect the effects of the crystallisation process on the surface defects, Figure 8 shows representative AFM images before and after crystallisation. The samples indented by 0.5 kg and 2.0 kg exhibit visual changes after the crystallisation. The indentation and the cracks are shallower, and the surface is notably smoother (Figure 8 a, b).

DISCUSSION

Our study shows that the defect sizes have a significant effect on the resulting BFS after crystallisation, and a single significant pairwise difference was found between the groups IND 0.2 and IND 2. A further analysis of the BFS via the survival rate (Figure 5) confirms that the only low-strength outliers come from the two groups with the largest defect sizes (IND 1 and IND 2). This suggests that while the crystallisation helps to mitigate smaller defects, the larger defects approach the limits of what the crystallisation mechanisms can remedy. This is consistent with previous work, where larger grinding defects lead to a decreased BFS [15, 27]. While Belli et al. 2019 reports that the crystallisation reduces the size of larger cracks introduced by machining, the reduced defects were still strength limiting (consistently with the results of Romanyk et al. 2019 [27]) as CAD/CAM machining damage often extends to at least 50 µm [29]. An important consideration in contextualising the current results with previous research is the fact that the expansion and the resulting material failure does not follow Griffith crack expansion where the initial crack size is the only relevant factor. The failure is rather a function of the crack size as well as the residual stress accumulated in the plastic zone of deformation [4, 7, 8]. The results from this study suggest that if the defects are sufficiently small enough, the crystallisation process can mitigate both the crack size and the residual stress up to a point where there is no significant difference in the BFS when compared to the control group.

Besides the restored BFS values, the post-crystallisation AFM pictures also suggest the altered surface of the indentation-defects (Figure 8). The indentation and the cracks are shallower, and the surface is noticeably smoother. Such an observation suggests that multiple material processes during crystallisation occur, as the growth of crystals and the viscous stage of glass could help to decrease the porosity of the material and to relax the residual stresses introduced during grinding.

The viscous flow of the glass and these microstructural changes can serve to reduce the crack size and residual stress, mitigating the surface defects and resulting strength degradation.

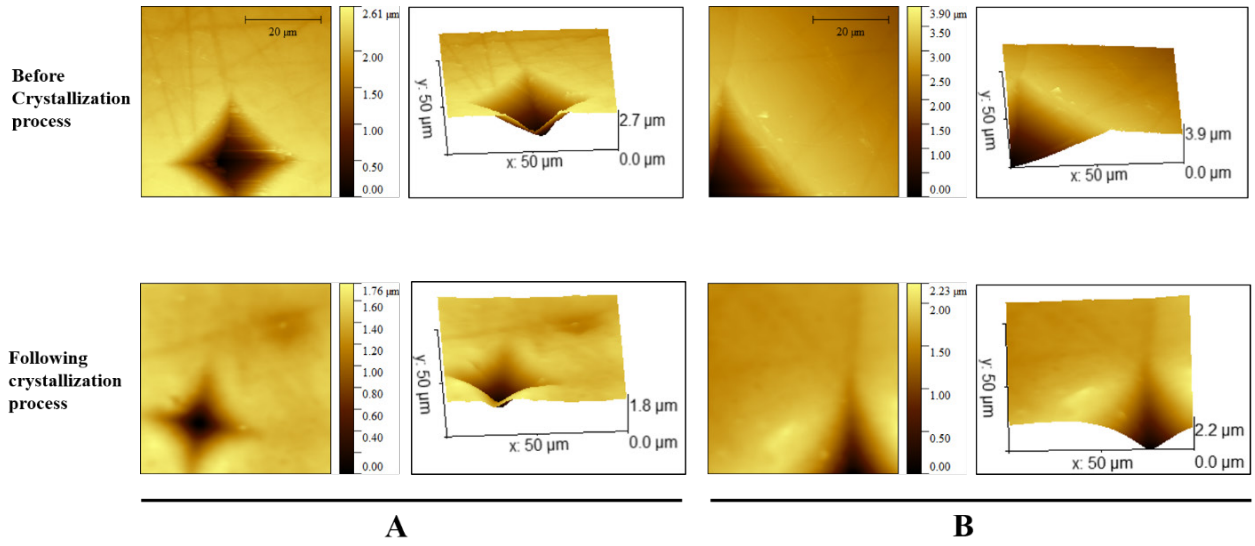

Figure 8. Atomic force microscopy (AFM) of the additional AFM group. (A) Sample with 0.5 kg indentation before and after crystallisation (B) Sample with 2 kg indentation before and after crystallisation. Both pictures demonstrate that the depth of the defect was decreased, while the borders of the diamond were smoothed out.

This is in agreement with Belli et al. 2019, where the reported strengthening effect and decreased crack dimension after the crystallisation process are attributed to the change of crystal structure and glass in the viscous flow cause the crack shrinkage [15]. Furthermore, the included XRD analysis pre- and post-crystallisation revealed cristobalite crystallisation on the surface of the IPS e.max CAD. This has been then suggested to potentially create beneficial compressive stresses shielding the defects and improving the strength. This study shows that the strength-limiting effects from small defects can be completely restored by recrystallisation.

The mechanism of the strength-limiting effects from the defects is well understood. A plastic zone of deformation and an associated stress field developed during the grinding process plays a crucial role for both the formation of cracks and their response to the subsequent loading [4]. While an elastic component is also involved during grinding and plays a role in the formation of cracks (e.g., suppressing the lateral cracks so that they only develop after the indenter is being removed), it is irrelevant for post-machining loading as it fully reverses after grinding. The post-machining strength, thus, depends on the residual stresses and the generated lateral and medial/radial cracks themselves [7]. Medial cracks do not extend back into the plastic deformation zone and together with the residual fields affect the resulting material strength [30]. Lateral cracks play a dominant role in the chipping of the material during the grinding process. The residual stresses then either help to stabilise or extend the cracks, dependent on the material and machining parameters (although the crack stabilising compressive stresses likely remain confined to a relatively thin layer) [15].

The positive effects of the crystallisation process presented in this and prior studies further motivate dental clinicians to minimise the severity of these defects (both cracks and residual stresses). Interestingly, Addison et al. 2012 showed that this cannot be achieved by simply using new burs rather than used ones (i.e., frequently changing burs does not help) as the surface roughness rather depends on a random selection of a bur and a random machining sequence [31]. Alao et al. 2017 reported that pre-crystallisation polishing is significantly more effective to post-crystallisation polishing in smoothing out the rough surface introduced by grinding; however, no strength data was collected preventing any further understanding of how the order of manufacturing operation would influence strength. Belli et al. 2019 then reported pre-crystallisation polishing as being more effective in terms of resulting strength measurements [15, 32]. Different crystallisation cooling rates have been investigated in Wendler et al. and Lohbauer et al. [33, 34]. Slower (soft) cooling under the transformation glass temperature led to reduced negative residual stresses. Furthermore, the direct contact of the firing pin with the glass ceramic developed localised residual stresses and also the fusion of the pin material into the ceramic. Thus, different firing setups were suggested. Namely, the use of fibrous pads or firing pastes seem to be good options to minimise the residual stresses near the contact with the ceramic material.

The limit of this study is that the indentation fracture mechanics assumes that the damage produced by grinding can be thought of as a single crack system produced by an indenter, the machining damage differs due to different configurations of the plastic deformation zone, associated cracks and the multiplicity of neighbouring damage sites [4]. Despite these discrepancies, the single indentation point has been shown as a reasonable model as it provides a qualitative description of the response of machining-induced cracks [4].

CONCLUSIONS

The current study has demonstrated that the crystallisation of the partially crystallised IPS e.max® CAD ceramic can heal small indentation defects, resulting in no statistical strength difference between the control group and groups with a small indentation. Post-processing steps are likely to modify the strength limiting defects and residual stress states. While the strengthening effects of the crystallisation have previously been reported, the post-healing defects are still strength-limiting. Our study shows that if the defects are sufficiently small enough, the process mitigates the strength-limiting effects up to the point where the microstructure governs the strength. Furthermore, the groups with larger defects suggest that the corresponding defects already approach the limits of the process and the post-processing defects are already becoming strength-limiting..

Acknowledgements

The authors would like to acknowledge the provision of laboratories and equipment through the University of Alberta School of Dentistry, and the financial support from Palacký University Olomouc. The publication was created with the support of a grant IGA_LF_2021_017. The authors acknowledge the financial support from the China Scholarship Council.

REFERENCES

1. Rekow E.D., Silva N.R.F.A., Coelho P.G., Zhang Y., Guess P., Thompson V.P. (2011): Performance of dental ceramics: Challenges for improvements. *Journal of Dental Research, 90*(8), 937-952. Doi:10.1177/0022034510391795
2. Mörmann W.H. (2006): The evolution of the CEREC system. *The Journal of the American Dental Association, 137*, 7S-13S. Doi:10.14219/jada.archive.2006.0398
3. Malkin S., Ritter J.E. (1989): Grinding mechanisms and strength degradation for ceramics. *Journal of*

Manufacturing Science and Engineering, 111, 167–174. Doi:10.1115/1.3188746
4. Marshall D.B., Evans A.G., Khuri Yakub B.T., Tien J.W., Kino G.S. (1983): The nature of machining damage in brittle materials. *Proceedings of the Royal Society of London. A. Mathematical and Physical Sciences, 385*(1789), 461-475. Doi:10.1098/rspa.1983.0023
5. Hu K.X., Chandra A. (1993): A fracture mechanics approach to modeling strength degradation in ceramic grinding processes. *Journal of Manufacturing Science and Engineering, 115*, 73–84. Doi:10.1115/1.2901642
6. Rice R.W., Mecholsky J.J. (1979). *The nature of strength controlling machining flaws in ceramics.* NBS Special Publication: The Science of Ceramic Machining and Surface Finishing II. US Government Printing Office.
7. Lawn B.R., Evans A.G., Marshall D.B. (1980): Elastic/Plastic Indentation Damage in Ceramics: The Median/Radial Crack System. *Journal of the American Ceramic Society, 63*(9-10), 574-581. Doi:10.1111/j.1151-2916.1980.tb10768.x
8. Marshall D.B., Lawn B.R., Evans A.G. (1982): Elastic/Plastic Indentation Damage in Ceramics: The Lateral Crack System. *Journal of the American Ceramic Society, 65*, 561–566. Doi:10.1111/j.1151-2916.1982.tb10782.x
9. Callister W.D., Rethwisch R.D. (2009). *Materials science and engineering: an introduction.* 8th ed. Wiley.
10. Marshall D.B., Lawn B.R. (1979): Residual stress effects in sharp contact cracking Part 1 Indentation fracture mechanics. *Journal of Materials Science, 14*, 2001-2012. Doi: 10.1007/BF00551043
11. Marshall D.B., Lawn B.R. (1980): Flaw Characteristics in Dynamic Fatigue: The Influence of Residual Contact Stresses. *Journal of the American Ceramic Society, 63*, 532–536. Doi:10.1111/j.1151-2916.1980.tb10759.x
12. Lawn B., Wilshaw R. (1975): Indentation fracture: principles and applications. *Journal of Materials Science, 10*, 1049–1081. Doi:10.1007/BF00823224
13. Lawn B.R., Swain M.V. (1975): Microfracture beneath point indentations in brittle solids. *Journal of Materials Science, 10*, 113-122. Doi:10.1007/BF00541038
14. Fasbinder D.J. (2010): Materials for chairside CAD/CAM restorations. *Compend Contin Educ Dent, 31*(9), 702-710.
15. Belli R., Lohbauer U., Goetz-Neunhoeffer F., Hurle K. (2019): Crack-healing during two-stage crystallization of biomedical lithium (di)silicate glass-ceramics. *Dental Materials, 35*(8), 1130-1145. Doi:10.1016/j.dental.2019.05.013
16. Ivoclar Vivadent. IPS e.max CAD Scientific Documentation. 2005.
17. Li R.W.K., Chow T.W., Matinlinna J.P. (2014): Ceramic dental biomaterials and CAD/CAM technology: State of the art. *Journal of Prosthodontic Research, 58*(4), 208-216. Doi:10.1016/j.jpor.2014.07.003
18. Willard A., Gabriel Chu T.M. (2018): The science and application of IPS e.Max dental ceramic. *The Kaohsiung Journal of Medical Sciences, 34*(4), 238-242. Doi:10.1016/j.kjms.2018.01.012
19. Sacher E., Franca R. (2018). *Dental Biomaterials*. 2nd ed. World Scientific.
20. Zhang Y., Kelly J.R. (2017): Dental Ceramics for Restoration and Metal Veneering. *Dental Clinics, 61*(4), 797-819. Doi:10.1016/j.cden.2017.06.005
21. Zarone F., Ferrari M., Mangano F.G., Leone R., Sorrentino R. (2016): "Digitally Oriented Materials": Focus on Lithium Disilicate Ceramics. *International Journal of Dentistry,* 2016, 1–10. Doi:10.1155/2016/9840594
22. Celtra Duo, Developed to make a difference, brochure for the dental laboratory. Dentsply Sirona. 2017
23. Kingery W.D., Bowen H.K., Uhlmann D.R. (1976). Thermal and compositional stresses in: Introduction to ceramics. 2nd ed. Wiley.
24. Ritzberger C., Schweiger M., Höland W. (2016): Principles of crystal phase formation in Ivoclar Vivadent glass-ceramics for dental restorations. *Journal of Non-Crystalline Solids, 432*, 137-142. Doi:10.1016/j.jnoncrysol.2015.04.034
25. Belli R., Wendler M., de Ligny D., Cicconi M.R., Petschelt A., Peterlik H., et al. (2017): Chairside CAD/CAM materials. Part 1: Measurement of elastic constants and microstructural characterization. *Dental Materials, 33*, 84–98. Doi:10.1016/j.dental.2016.10.009
26. Zhang P., Li X., Yang J., Xu S. (2014): The crystallization and microstructure evolution of lithium disilicate-based glass-ceramic. *Journal of Non-Crystalline Solids, 392–393*, 26–30. Doi:10.1016/j.jnoncrysol.2014.03.020
27. Romanyk D.L., Martinez Y.T., Veldhuis S., Rae N., Guo Y., Sirovica S., et al. (2019): Strength-limiting damage in lithium silicate glass-ceramics associated with CAD–CAM. *Dental Materials, 35*, 98–104. Doi:10.1016/j.dental.2018.11.004
28. Romanyk D.L., Guo Y., Rae N., Veldhuis S., Sirovica S., Fleming G.J., et al. (2020): Strength-limiting damage and its mitigation in CAD-CAM zirconia-reinforced lithium-silicate ceramics machined in a fully crystallized state. *Dental Materials, 36*, 1157–1565. Doi:10.1016/j.dental.2020.09.012
29. Sindel J., Petschelt A., Grellner F., Dierken C., Greil P. (1998): Evaluation of subsurface damage in CAD/CAM machined dental ceramics. *Journal of Materials Science: Materials in Medicine, 9*(5), 291-295. Doi:10.1023/A:1008812929476
30. Evans A.G., Wilshaw T.R. (1976): Quasi-static solid particle damage in brittle solids-I. Observations analysis and implications. *Acta Metallurgica, 24*, 939–956. Doi:10.1016/0001-6160(76)90042-0
31. Addison O., Cao X., Sunnar P., Fleming G.J.P. (2012): Machining variability impacts on the strength of a "chair-side" CAD-CAM ceramic. *Dental Materials, 28*, 880–887. Doi:10.1016/j.dental.2012.04.017
32. Alao A.R., Stoll R., Song X.F., Abbott J.R., Zhang Y., Abduo J., et al. (2017): Fracture, roughness and phase transformation in CAD/CAM milling and subsequent surface treatments of lithium metasilicate/disilicate glass-ceramics. *Journal of the Mechanical Behavior of Biomedical Materials, 74*, 251-260.Doi:10.1016/j.jmbbm.2017.06.015
33. Wendler M., Belli R., Lohbauer U. (2019): Factors influencing development of residual stresses during crystallization firing in a novel lithium silicate glass-ceramic. *Dental Materials, 35*, 871–882. Doi:10.1016/j.dental.2019.03.002
34. Lohbauer U., Wendler M., Rapp D., Belli R. (2019): Fractographic analysis of lithium silicate crown failures during sintering. *SAGE Open Medical Case Reports, 7*, 1–8. Doi:10.1177/2050313x19838962